Research Article | Vol. 25, No. 13 | 26 Jun 2017 | OPTICS EXPRESS 14996
Optics EXPRESS

An analytical model for light backscattering by coccoliths and coccospheres of *Emiliania huxleyi*

GEORGES FOURNIER[1,*] AND GRIET NEUKERMANS[2]

[1]*DRDC Valcartier Research Laboratory, Québec, Québec, G3J1X5, Canada*
[2]*Takuvik Joint International Laboratory, CNRS and Université Laval, Québec, G1V 0A6, Canada*
[*]*georges.fournier@drdc-rddc.gc.ca*

Abstract: We present an analytical model for light backscattering by coccoliths and coccolithophores of the marine calcifying phytoplankter *Emiliania huxleyi*. The model is based on the separation of the effects of diffraction, refraction, and reflection on scattering, a valid assumption for particle sizes typical of coccoliths and coccolithophores. Our model results match closely with results from an exact scattering code that uses complex particle geometry and our model also mimics well abrupt transitions in scattering magnitude. Finally, we apply our model to predict changes in the spectral backscattering coefficient during an *Emiliania huxleyi* bloom with results that closely match in situ measurements. Because our model captures the key features that control the light backscattering process, it can be generalized to coccoliths and coccolithophores of different morphologies which can be obtained from size-calibrated electron microphotographs. Matlab codes of this model are provided as supplementary material.

OCIS codes: (280.1350) Backscattering; (010.4458) Oceanic scattering ; (120.5700) Reflection ; (240.5770) Roughness ; (290.5825) Scattering theory ; (290.5850) Scattering, particles ; (290.5880) Scattering, rough surfaces; (330.6180) Spectral discrimination; (010.4450) Oceanic optics.

References and links

1. C. J. O'Brien, M. Vogt, and N. Gruber, "Global coccolithophore diversity: Drivers and future change," Prog. Oceanogr. **140**, 27–42 (2016).
2. M. D. Iglesias-Rodríguez, C. W. Brown, S. C. Doney, J. Kleypas, D. Kolber, Z. Kolber, P. K. Hayes, and P. G. Falkowski, "Representing key phytoplankton functional groups in ocean carbon cycle models: Coccolithophorids," Global Biogeochem. Cycles **16**(4), 47 (2002).
3. W. Balch, H. Gordon, B. Bowler, and E. Booth, "Calcium carbonate measurements in the surface global ocean based on Moderate-Resolution Imaging Spectroradiometer Data," J. Geophys. Res. **110**(C7), C07001 (2005), doi:10.1029/2004JC002560.
4. H. R. Gordon, G. C. Boynton, W. M. Balch, S. B. Groom, D. S. Harbour, and T. J. Smyth, "Retrieval of coccolithophore calcite concentration from SeaWiFS imagery," Geophys. Res. Lett. **28**(8), 1587–1590 (2001).
5. K. Voss, W. Balch, and K. Kilpatrick, "Scattering and attenuation properties of Emiliania huxleyi cells and their detached coccoliths," Limnol. Oceanogr. **43**(5), 870–876 (1998).
6. W. M. Balch, P. M. Holligan, S. G. Ackleson, and K. J. Voss, "Biological and optical properties of mesoscale coccolithophore blooms in the Gulf of Maine," Limnol. Oceanogr. **36**(4), 629–643 (1991).
7. E. M. Purcell and C. R. Pennypacker, "Scattering and absorption of light by nonspherical dielectric grains," Astrophys. J. **186**, 705–714 (1973).
8. H. R. Gordon and T. Du, "Light scattering by nonspherical particles: application to coccoliths detached from *Emiliania huxleyi*," Limnol. Oceanogr. **46**(6), 1438–1454 (2001).
9. P.-W. Zhai, Y. Hu, C. R. Trepte, D. M. Winker, D. B. Josset, P. L. Lucker, and G. W. Kattawar, "Inherent optical properties of the coccolithophore: *Emiliania huxleyi*," Opt. Express **21**(15), 17625–17638 (2013).
10. M. Jonasz and G. Fournier, *Light Scattering by Particles in Water: Theoretical and Experimental Foundations* (Academic, 2007), *pp. 117–121*
11. G. Fournier, "Backscatter corrected Fournier-Forand phase function for remote sensing and underwater imaging performance evaluation," in *Current Research on Remote Sensing, Laser Probing, and Imagery in Natural Waters*, I. M. Levin, G. D. Gilbert, V. I. Haltrin, C. C. Trees, eds., Proc. SPIE 6615, (2007).
12. G. R. Fournier, V. Sanjuan-Calzado, and C. Trees, "Implications of a new phase function for autonomous underwater imaging," Proc. SPIE **VI**, 911119 (2014).
13. H. R. Gordon, "Backscattering of light from disk-like particles with aperiodic angular fine structure," Opt. Express **15**(25), 16424–16430 (2007).

#287035 https://doi.org/10.1364/OE.25.014996
Journal © 2017 Received 23 Feb 2017; revised 12 Apr 2017; accepted 19 Apr 2017; published 21 Jun 2017

Optics EXPRESS

14. H. R. Gordon, "Backscattering of light from disklike particles: is fine-scale structure or gross morphology more important?" Appl. Opt. **45**(27), 7166–7173 (2006).
15. H. C. Van de Hulst, *Light Scattering by Small Particles* (Wiley, 1957), *pp.111–112*
16. B. Hapke, *Theory of reflectance and emittance spectroscopy*, (Cambridge University, *2012), pp.105–109.*
17. E. Schoenberg, "Handb.," Astrophysik **2**, 255 (1929).
18. G. Neukermans and G. Fournier, "Qbb_Ehux: Backscattering efficiency factors for coccoliths and coccospheres of *Emiliania huxleyi*" GitHub (2017), [retrieved 13 April 2017] https://doi.org/10.5281/zenodo.545645.
19. E. D. Palik, *Handbook of Optical Constants of Solids* (Academic, 1998), Volume 3, pp. 704–708.
20. D. Stramski, A. Bricaud, and A. Morel, "Modeling the inherent optical properties of the ocean based on the detailed composition of the planktonic community," Appl. Opt. **40**(18), 2929–2945 (2001).
21. A. R. Neeley, S. A. Freeman, and L. A. Harris, "Multi-method approach to quantify uncertainties in the measurements of light absorption by particles," Opt. Express **23**(24), 31043–31058 (2015).
22. E. Aas, "Refractive index of phytoplankton derived from its metabolite composition," J. Plankton Res. **18**(12), 2223–2249 (1996).
23. D. Risović, "Two-component model of sea particle size distribution," Deep-Sea Res. **40**(7), 1459–1473 (1993).
24. H. R. Gordon, T. J. Smyth, W. M. Balch, G. C. Boynton, and G. A. Tarran, "Light scattering by coccoliths detached from Emiliania huxleyi," Appl. Opt. **48**(31), 6059–6073 (2009).
25. E. Paasche, "A review of the coccolithophorid *Emiliania huxleyi* (Prymnesiophyceae), with particular reference to growth, coccolith formation, and calcification-photosynthesis interactions," Phycologia **40**(6), 503–529 (2001).
26. B. Delille, J. Harlay, I. Zondervan, S. Jacquet, L. Chou, R. Wollast, R. G. Bellerby, M. Frankignoulle, A. V. Borges, U. Riebesell, and J. P. Gattuso, "Response of primary production and calcification to changes of pCO2 during experimental blooms of the coccolithophorid *Emiliania huxleyi*," Global Biogeochem. Cycles **19**(2), GB2023 (2005), doi:10.1029/2004GB002318.
27. IOCCG, Remote sensing of inherent optical properties: fundamentals, tests of algorithms, and applications. In Z. Lee [ed.], Reports of the International Ocean-Colour Coordinating Group, No. 5, IOCCG, Dartmouth, Canada (2006).
28. M. Abramowitz and I. A. Stegun, *Handbook of mathematical Functions* (National Bureau of Standards, 1964), pp. 228–229.

1. Introduction

Coccolithophores are a group of phytoplankton distinctive by their production of elegantly sculpted calcite plates, coccoliths, which are organized around each living cell as an outer covering forming the so-called coccosphere. Coccolithophores thrive in a wide range of marine environments from subtropical gyres to subpolar waters [1]. They are major calcifiers in the ocean and play a key role in the oceanic carbon cycle [2]. Among the estimated 200 species of coccolithophores, the species *Emiliania huxleyi* (*Ehux*) is one of the most ubiquitous (Fig. 1). This species forms intense blooms in the temperate oceans and seas, shedding its coccoliths at the final bloom stages. These scatter so much sunlight that seawater turns bright milky-turquoise making blooms easily detectable by the naked eye and from space [3, 4].

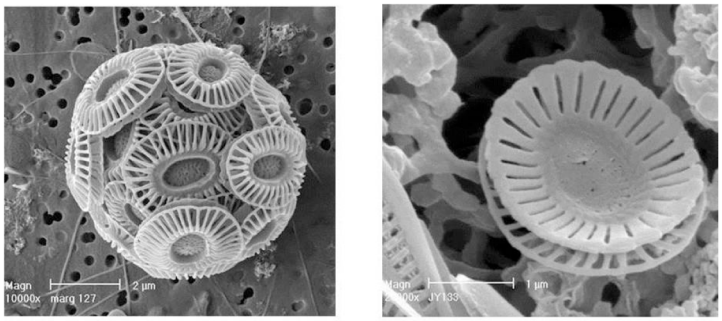

Fig. 1. Scanning Electron Micrograph of Emiliania huxleyi (Dr. Jeremy Young, University College London, London, with permission)

Understanding the light scattering properties of *Ehux'* coccospheres and coccoliths is of key importance for the monitoring of this species from space borne or in situ optical

Optics EXPRESS

measurements. Previous experimental studies have obtained the scattering properties of *Ehux* in laboratory cultures [5] as well as in natural waters [6]. The most commonly used approach in optical oceanography when modelling the angular light scattering coefficients is Mie theory, which treats marine particles as homogeneous spheres. However, scattering by irregularly shaped particles with complex morphologies such as coccoliths and coccospheres is significantly different from that of homogeneous spheres, especially in the back-direction. One of the frequently used methods to compute light scattering from arbitrary shaped particles is the discrete dipole approximation, DDA [7], which has been applied to coccoliths by Gordon and Du [8]. They showed that, in contrast to the total scattering coefficient, the backscattering coefficient and its spectral variation was strongly dependent on coccolith morphology due to multiple reflections within the particle. More recently, Zhai et al. [9] applied the DDA approach to coccospheres and coccoliths with a very realistic morphology and demonstrated in great detail differences in light scattering, absorption and depolarization ratio. However, DDA approaches are computationally demanding which hampers their practical application to real-world problems in optical oceanography.

The goal of the present study is to develop and test a generic analytical model for light scattering by coccoliths and coccospheres of arbitrary morphology. First, we develop the model based on the separation of the effects of diffraction, refraction, and reflection on light scattering. Next, we compare our model with the exact solutions of light scattering obtained from DDA, and lastly, we compute changes in spectral backscattering during a hypothetical *Ehux* bloom in which *Ehux* sheds its attached liths.

2. Analytical model description

The diameter of *Ehux'* coccoliths and coccospheres is typically on the order of 2.5 microns and 6 microns respectively. Therefore these particles can be considered to be optically large. Moreover, these particles are made of calcite with an index of refraction of 1.64 which gives a relative index with respect to seawater of 1.22, small enough to be in the range of validity of the anomalous diffraction approximation. These conditions allow separation of the effects of diffraction, refraction, and reflection on scattering as follows [10–12]:

$$\overline{\sigma}_{bb} = \overline{\sigma}_g \left[Q_{bdiff} + Q_{brefr} + Q_{brefl} \right] = \overline{\sigma}_g \left[Q_{bdiff} + Q_{brefr} + \omega F_{brefl} \right] \tag{1}$$

$\overline{\sigma}_{bb}$ is the mean backscattering cross-section while $\overline{\sigma}_g$ is the mean projected surface area of an individual particle averaged over a uniform random distribution of particle orientation and the Q factors are the scattering efficiency factors due to diffraction, refraction, and reflection. For optically large particles and for scattering in the back direction only the reflection term is significant, therefore:

$$\overline{\sigma}_{bb} = \overline{\sigma}_g \left[\omega F_{brefl} \right] \tag{2}$$

where ω is the total reflection integrated over all angles while F_{brefl} is the fraction of the scattering due to reflection that lies in the backscattering hemisphere. The reflection component ω can be further broken down into a specular reflection component coming from the smooth part ω_{bsm} of the particle surface and a diffuse reflection component originating from the rough part of the particle surface ω_{brg}, thus $\omega = \omega_{bsm} + \omega_{brg}$. These reflection components have very different angular behaviour. The smooth specular part heavily favours scattering in the forward hemisphere while the rough diffuse scattering is concentrated largely in the backward hemisphere. In our original formulation [10–12] we noted that the total reflection effect governed by ω could be modeled as a linear combination of the two types of scattering controlled by a simple mixing coefficient R:

Optics EXPRESS

$$Q_{brefl} = \omega_{bsm}\left(1 - RF_{rg}\right) + \omega_{brg} RF_{rg} \tag{3}$$

We did, however, not specify how one should compute the value of R for a given type of particle. In Eq. (3) F_{rg} is the maximum fraction of the projected area of the particle that can become rough. In what follows, we will derive formulas for R, ω_{bsm}, ω_{brg} and F_{rg} for the specific case of a coccolith particle. We will use the coccolith morphological characteristics as defined by Zhai et al. [9] and shown in Fig. 2.

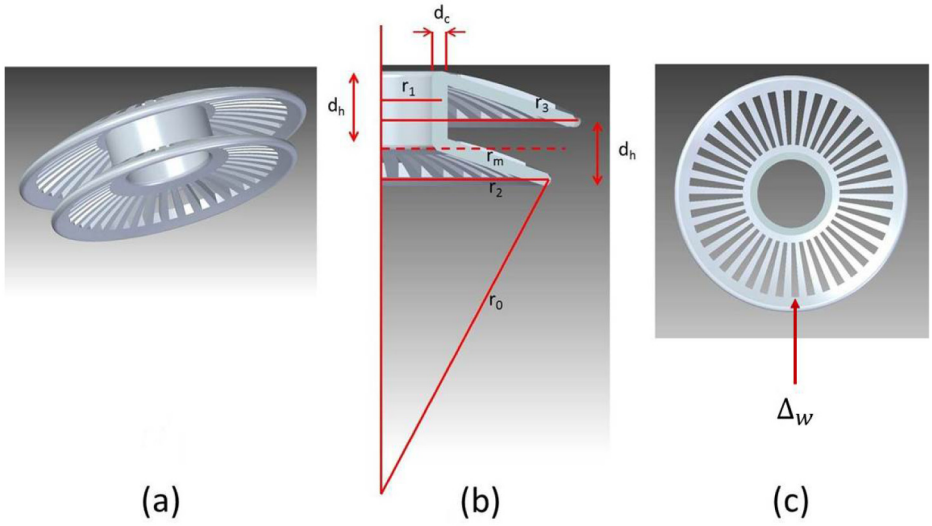

Fig. 2. Realistic model of an *Emiliania huxleyi* coccolith used by Zhai et al. [9]

With reference to Fig. 2(b) r_0 is the radius of the naked coccolithophore core that the coccolith is attached to and all the other dimensions are related to it as follows [9]:

$$\frac{r_1}{r_0} = 0.18,\quad \frac{r_2}{r_0} = 0.46,\quad \frac{r_3}{r_0} = 0.54,\quad \frac{r_m}{r_0} = 0.50,\quad \frac{d_c}{r_0} = 0.07,\quad \frac{d_h}{r_0} = 0.18$$

The outer radius of a coccosphere with a core of radius r_c covered in a single layer of coccoliths is therefore

$$r_{tot} = r_c + d_h + d_c = 1.215\, r_0 \tag{4}$$

Both the coccolith distal and proximal sheets have 40 wedge shaped openings in line with one another. As noted in a previous set of papers [13, 14] on scattering by coccolithophores, a sharp increase in the backscatter occurs just when the open gaps in the distal and proximal sheets of the coccoliths (spoke gap width Δ_w, see Fig. 2(c)) which vary as a function of radial distance become larger than a quarter of the wavelength $\lambda/4$. The transition point between average index (smooth) effect reflection and structured scattering (rough reflection) occurs at the radius r_{tr} when Δ_w is equal to or larger than $\lambda/4$ [15–17]. Assuming N pairs of wedges and equally wide solid spokes this leads to the following critical size for the beginning of the smooth to rough reflection transition:

$$\Delta_w = \frac{\lambda}{4} = \frac{2\pi r_{tr}}{2N} \tag{5}$$

$$\frac{x_{tr}}{2N} = \frac{1}{4} \rightarrow x_{tr} = \frac{N}{2} \tag{6}$$

Optics EXPRESS

r_{tr} is the radius at which the spoke gap gets larger than $\lambda/4$ while x_{tr} is the corresponding dimensionless size parameter.

As the coccolith becomes larger, the portion of the open wedges where the gap exceeds a lateral dimension of $\lambda/4$ increases. We denote the maximum radius at which the gaps start to appear as r_{mxs} and the minimum radius at which they disappear as r_{mns} with corresponding size parameters of x_{mxs} and x_{mns}. The fraction R of the area of the spokes and gaps that contribute to rough (i.e Lambertian scattering) versus smooth scattering is therefore simply given as:

$$R = \frac{x_{mxs}^2 - x_{tr}^2}{x_{mxs}^2 - x_{mns}^2}, \quad x_{mns} \le x_{tr} \le x_{mxs} \tag{7}$$

Rearranging terms and substituting Eq. (6) we get:

$$R = \frac{1-\left(\frac{x_{tr}}{x_{mxs}}\right)^2}{1-\left(\frac{x_{mns}}{x_{mxs}}\right)^2} = \frac{1-\left(\frac{N/2}{x_{mxs}}\right)^2}{1-\left(\frac{x_{mns}}{x_{mxs}}\right)^2} \tag{8}$$

And outside the bounds of the transfer region we have:

$$x_{tr} \le x_{mns} \rightarrow R = 1$$
$$x_{tr} \ge x_{mxs} \rightarrow R = 0$$

Another parameter we need to evaluate in Eq. (3) is the maximum fraction of the total projected area of the coccolith that can become rough, F_{rg}. Let x_{lith} be the dimensionless size parameter corresponding to the maximum transverse radius of the coccolith disk, then F_{rg} can be expressed as:

$$F_{rg} = \frac{x_{mxs}^2 - x_{mns}^2}{x_{lith}^2} \tag{9}$$

Next, we evaluate the backscatter reflections for smooth and rough surfaces, ω_{bsm} and ω_{brg}, respectively. For smooth surfaces the backscatter reflection is given by [10]:

$$\omega_{bsm} = 2\pi \int_{\pi/2}^{\pi} \left(\frac{1}{4\pi}\right) \sum_i \left|r_i(\theta)\right|^2 \sin\theta \, d\theta \tag{10}$$

In the expression above $\left|r_i(\theta)\right|^2$ is the Fresnel reflection coefficient for each surface i of the particle. By carrying out the integrals in Eq. (10), we obtain for each surface i the backscatter reflection coefficients for polarizations perpendicular and parallel to the scattering plane.

$$\omega_{bi\perp}(n) = \frac{3n^4 - 16n^3 + 12n^2 - 1 + 2\left(2n^2 - 1\right)^{3/2}}{6\left(n^2 - 1\right)^2} \tag{11}$$

The formula for the backscattering parallel to the plane is very long and complex. Fortunately the result can be efficiently approximated to better than 0.2% relative error as follows:

$$\omega_{bi\parallel}(n) = \left[(3 - \ln 16) + \frac{37}{40}\left(\frac{n-1}{n+1}\right)\right]\omega_{b\perp} \tag{12}$$

$$\omega_{bsm} = \sum_i \omega_{bi}(n) = \sum_i \frac{\omega_{bi\perp} + \omega_{bi\parallel}}{2} \tag{13}$$

Optics EXPRESS

To evaluate ω_{brg} we proceed a little differently. We first evaluate the total reflection over all scattering angles:

$$\omega_t = 2\pi\int_0^{\pi}\left(\frac{1}{4\pi}\right)\sum_i |r_i(\theta)|^2 \sin\theta\, d\theta \tag{14}$$

The formulas for the reflections for polarizations perpendicular and parallel to the scattering plane for each surface *i* were first given in [10–12]. These have been corrected here for typos:

$$\omega_{i\perp} = \frac{(3n+1)(n-1)}{3(n+1)^2} \tag{15}$$

$$\omega_{i\parallel} = \frac{1}{(n^2+1)^3(n^2-1)^2}\left\{ (n^4-1)(n^6-4n^5-7n^4+4n^3-n^2-1) + 2n^2\left[(n^2-1)^4 \ln\left(\frac{n-1}{n+1}\right) + 8n^2(n^4+1)\ln(n)\right]\right\} \tag{16}$$

$$\omega_t = \sum_i \omega_i(n) = \sum_i \frac{\omega_{i\perp}(n)+\omega_{i\parallel}(n)}{2} \tag{17}$$

Note that the fundamental reason we can use the same formulas for the reflectivity of the front and back surfaces is that we are dealing with flat disks and the surface elements facing each other across the thickness of the disk are at the same relative angle with respect to the light ray. This situation is fundamentally different than that of the spheres discussed in [10].

The angular reflectivity distribution of a sphere with a rough diffuse surface is given by [15–17]

$$p_{rg}(\theta) = \omega_t\left(\frac{2}{3\pi^2}\right)(\sin\theta - \theta\cos\theta) \tag{18}$$

Integrating Eq. (18) over angles in the back hemisphere we get:

$$\omega_{brg} = \left(\frac{5}{6}\right)\omega_t \tag{19}$$

Equations (10)–(19) are valid for each surface reflection and for the sum of these reflections in the case that the material is not absorbing. These can be modified to account for a complex index $m = n - ik$ as outlined in the appendix. The change in reflectivity induced by the presence of k can be accounted for by using an effective real index and the absorption losses between the multiple surfaces can be computed directly.

From Eqs. (10)–(19) we can readily obtain the complete expression for the ratio of rough to smooth backscattering as a function of index of refraction:

$$\frac{\omega_{brg}}{\omega_{bsm}} = \left(\frac{5}{6}\right)\frac{\omega_t\, 6(n^2-1)^2}{3n^4-16n^3+12n^2-1+2(2n^2-1)^{3/2}}\left[\frac{2}{1+(3-\ln 16)+\frac{37}{40}\left(\frac{n-1}{n+1}\right)}\right] \tag{20}$$

This ratio is depicted in Fig. 3. For a calcite coccolith, the index relative to water is 1.20 and the ratio in Eq. (20) is 7.92. If we multiply this ratio by the maximum fraction of the coccolith surface which is rough we obtain the asymptotic value of the backscattering ratio at short wavelengths. The long wavelength asymptote is a perfectly smooth surface.

Optics EXPRESS

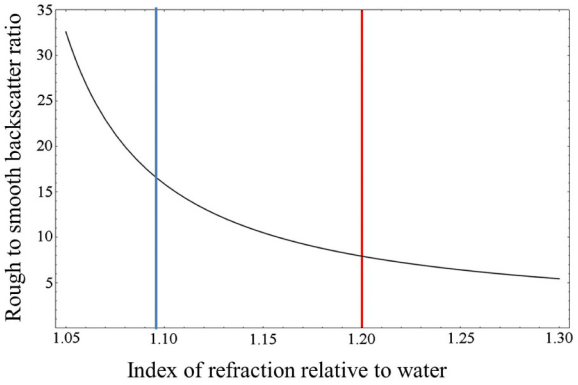

Fig. 3. Rough to smooth backscatter ratio as a function of index of refraction. The red line is the index of calcite relative to water used by Zhai et al. [9] in their model and for comparison the blue line is the index of silica (1.094) which forms diatom frustules

According to our analysis, the behavior of the backscattering cross section for coccoliths as a function of wavelength will be as follows. In the long wavelength limit the whole surface of the particle appears perfectly smooth since asperities or holes will be smaller than $\lambda/4$:

$$\overline{\sigma}_{bb} = \overline{\sigma}_g \ \omega_{bsm} \tag{21}$$

As the wavelength gets shorter some parts of the surface will start to appear as rough and the backscatter cross-section will increase quickly. When the wavelength gets short enough that all the asperities and holes are larger than $\lambda/4$ the backscatter cross-section will reach a maximum value given by

$$\overline{\sigma}_{bb} = \overline{\sigma}_g \ \omega_{bsm} \left[\left(1 - F_{rg}\right) + \frac{\omega_{brg}}{\omega_{bsm}} F_{rg} \right] \tag{22}$$

The analytical model presented above has been implemented in Matlab and the code is provided as supplementary information to this paper [18]. It provides the backscattering efficiency factors of coccoliths and coccolithophores derived from Eq. (3) for real and complex index of refraction.

3. Comparison of the analytical model with the exact scattering solution

Zhai et al. [9] report results for the backscattering ratio b_{bb}/b and the total scattering efficiency Q_{scat} for *Ehux'* coccoliths and coccolithophores. By multiplying these we obtain the backscattering efficiency $Q_{bscat} \cong Q_{brefl}$

$$\frac{b_{bb}}{b} = \frac{Q_{bscat}}{Q_{scat}} \cong \frac{Q_{brefl}}{Q_{scat}} \rightarrow Q_{brefl} \cong Q_{scat} \left(\frac{b_{bb}}{b} \right) \tag{23}$$

In Fig. 4(a) we compare the backscattering efficiency of coccoliths obtained by our model with results obtained by Zhai et al. [9] for the case of a coccolith with a real index of refraction of 1.2 with no absorption and for the corresponding case of absorption with $k = 0.01$.

Zhai et al. [9]'s original data was plotted as a function of the spherical volume equivalent radius. While this is adequate for the nearly spherical coccolithophores, it is much is more problematic for randomly oriented disks where the geometric cross-section is very different for the same volume. We have therefore chosen to use instead an equivalent disk thickness size parameter for the coccoliths. This equivalent disk contains the same volume $V_c(r_0)$ as the coccoliths including the empty spaces between the spokes (see Matlab code provided as

Optics EXPRESS

supplementary material [18]) and has the same mean radius r_m. This automatically defines the equivalent thickness size parameter. The total equivalent thickness t_t of the combined distal t_d and proximal t_p sheet (see Fig. 1A in the appendix) is given by:

$$t_t = \frac{V_c(r_0)}{\pi r_m^2} = t_d + t_p \rightarrow t_t = \frac{2\pi(t_d + t_p)}{\lambda} \tag{24}$$

Treating this structure as a set of two very closely spaced disks allows us to properly model the distal and proximal sheets with their four reflective interfaces.

The sharp transition from smooth to rough reflectivity is clearly seen in both the exact case and our approximate model (Fig. 4). The reduction in the backscattering seen in the case of finite absorption is simply due to the reduction in signal returned from the three back surfaces due to absorption. As expected, the proportion of the reduction can be seen to increase as a function of the coccolith thickness.

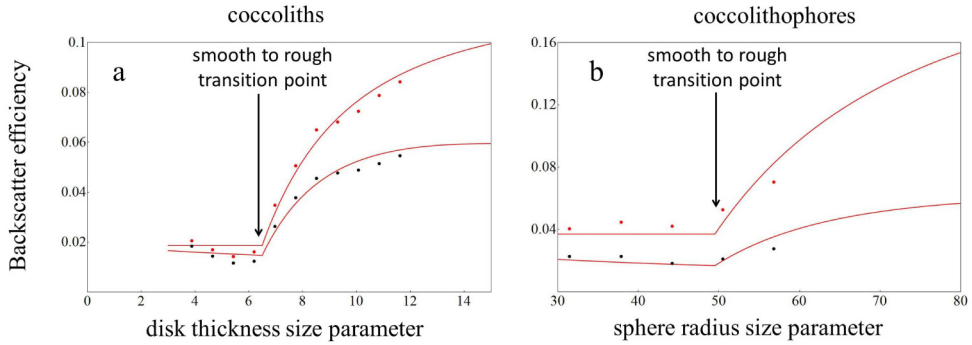

Fig. 4. Backscatter efficiency of coccoliths (a) and coccolithophores (b). Points are the results from the exact ADDA code of Zhai et al. [9] with no absorption k = 0.0 (red) and with and absorption of k = 0.01 (black). The red lines are the corresponding results from the analytical model.

In Fig. 4(b) we compare the backscattering efficiency of coccospheres obtained by our model with results obtained by Zhai et al. [9]. The transition to rough backscattering is also observed here but only at the largest particle sizes that were analyzed by Zhai et al. [9]. Since coccoliths are smaller than coccospheres it should be noted that the coccosphere size parameter where this transition starts is also exactly where the gaps in the coccoliths becomes $\lambda/4$. Note that in this case there are eight reflecting surfaces needed to account for both the coccoliths covering the front of the coccosphere and those covering the back of the coccosphere which doubles the value of the backscattering efficiency when there is no absorption. When there is absorption, the backscattering efficiency is halved since very little signal comes back from the surfaces on the back of the coccosphere because of the long absorbing path through the core material.

We are now in a position to discuss the spectral behavior expected for backscatter efficiency for coccoliths and coccospheres. For calcite the absorption is negligible even in the far UV [19]. We therefore expect that the spectral behavior of the individual detached coccoliths will show a sharp transition upwards in the blue and UV region. This spectral signature is shown in Fig. 5(a) for a coccolith with a diameter of 2.5 micron and in Fig. 5(b) for a coccosphere of 6.25 micron diameter. The transition wavelength is around 550 nm. For larger coccoliths this transition will move to longer wavelength in a manner directly proportional to the size. In other words the transition size parameter is constant assuming the whole relative geometrical structure of the coccoliths stays the same. Given a size distribution

Optics EXPRESS

of coccoliths one can directly estimate the spectral signature of that distribution. In general those signatures will show a smooth rise toward the UV.

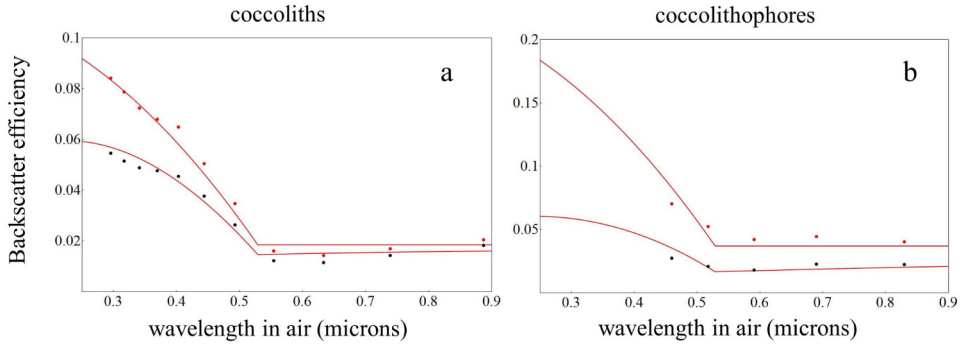

Fig. 5. (a) Backscatter efficiency of a 2.5 micron diameter coccolith as a function of wavelength. (b) Backscatter efficiency of a 6.25 micron diameter coccosphere as a function of wavelength. Points are from the code of Zhai et al. [9] for coccospheres with no absorption k = 0.0 (red) and with an absorption of k = 0.01 (black). The red lines are the corresponding results from the analytical model.

The situation is somewhat different in the case of coccospheres. The core has a distinct spectral signature [20, 21] that will modulate the backscattering by a factor of up to two by masking the reflection from the coccoliths covering the back of the coccosphere (see appendix). This spectral modulation in signature may have the potential to be used to estimate the ratio of free coccoliths to coccolithophores.

Finally, contribution of the naked cores can be evaluated using either an anomalous diffraction model or Mie scattering code. Their backscatter contribution is however much smaller than the contribution of the calcite coccosphere since they have a single reflecting surface involved and its inherent reflectivity is much smaller given the average relative index is 1.04 [22].

4. Comparison of the analytical model with laboratory and *in situ* results

To compare our results with experimental measurements we used the mean size distribution and the spectral absorption values given in [20, 21]. We used a shifted Gamma function size distribution model which has been argued to be a better fit than Log-Normal distributions for real biological size distributions [23].

$$r \le r_{\min} \rightarrow p(r) = 0, \quad r > r_{\min} \rightarrow p(r) = \beta^2 (r - r_{\min}) e^{-\beta(r - r_{\min})} \tag{25}$$

For this distribution the parameters are related to the mean particle size μ and the standard deviation of the distribution σ as follows.

$$\beta = \frac{\sqrt{2}}{\sigma}, \quad r_{\min} = \mu - \sqrt{2}\sigma \tag{26}$$

Equations (25)–(26) are sufficient to model coccoliths but to model correctly the geometric cross-section of coccolithophores we need to account for coccospheres that can be composed of several layers of coccoliths.

$$r_s = r_c + (O_{vl} - 1)\Delta r_l \tag{27}$$

O_{vl} is an overlap factor that is a measure of the added size due to the presence of coccoliths attached to the coccosphere. In the present model we are assuming that the coccoliths proximal sheets are attached to the lower layer or the core in the case of the first layer. It is this lower layer that is completely covered in coccoliths and is used in the next

Optics EXPRESS

section to evaluate the number of coccoliths per layer. To be consistent with the model used by Zhai et al. [9] we have

$$\Delta r_l = d_h + d_c = 0.25\, r_o \tag{28}$$

The results from the laboratory measurement for coccoliths and coccolithophores of Voss et al. [5] along with the in situ measurements taken by Gordon et al. [24] are compared in Fig. 6 below. The agreement is well within experimental error in all cases.

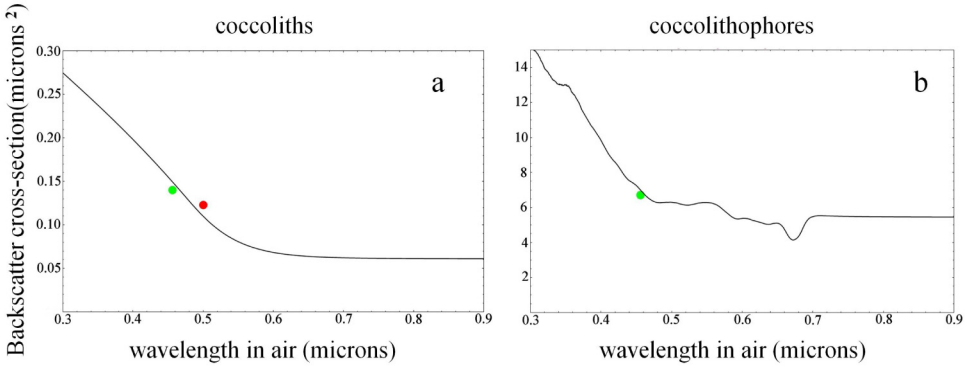

Fig. 6. Backscatter cross-section for (a) a coccolith population with mean diameter of 2.4 microns and with a size distribution standard deviation of 0.23 microns and for (b) a coccolithophore population with mean naked core diameter of 5.2 microns and an overlap factor of 2.The solid lines are theory. The green dots are the laboratory data of Voss et al. [5] and the red dot is the field data of Gordon et al. [23].

5. Predicted changes in spectral backscattering during a coccolithophore bloom

In what follows, we simulate changes in spectral backscattering during a hypothetical *Ehux* bloom in which *Ehux* sheds its attached liths for example due to nutrient limitation [5, 25, 26]. Given both the pure coccosphere spectrum and the pure coccolith spectrum, they can be mixed linearly to describe the evolution of a bloom. The backscattering cross-section for a mix of liths and spheres can be written as:

$$\sigma_{bloom}(\lambda) = (1 - F_s) O_{vl} Q_{bs}(\lambda) \sigma_{gs} + N_l F_s Q_{bl}(\lambda) \overline{\sigma}_{gl} + F_s Q_{bc} \sigma_{gc} \tag{29}$$

N_l is the number of liths covering the coccosphere, O_{vl} is the number of layers of liths covering the coccosphere and F_s is the fraction of the liths that have been shed. Multiplying the backscattering cross-section $Q_{bs}(\lambda)\sigma_{bs}$ x sigma bs by the overlap factor O_{vl} is required to properly account for the increase in the number of reflecting surfaces covering the coccosphere. The last term is the backscattering from the naked core surface which turns out to be negligible in practice when compared to the other terms because its small relative index leads to very small reflection efficiency.

To compute σ_{bloom} we need to evaluate the geometric cross-section of randomly oriented convex volumes which is given by one quarter of their respective surface areas [15]. For the coccospheres we simply have:

$$\sigma_{gs} = \pi r_s^2 = \pi \left[r_c + (O_{vl} - 1) \Delta r_l \right]^2 \tag{30}$$

Δr_l is the increase in radius of the coated coccosphere per layer of coccoliths attached to its core defined in Eq. (27).

For the coccoliths which we represent as an equivalent disks we have:

Optics EXPRESS

$$\overline{\sigma}_{gl} = \left(\frac{1}{4}\right)\left(2\pi r_m^2 + 2\pi r_m t_t\right) = \left(\frac{\pi r_m^2}{2}\right)\left(1 + f_t\right) \tag{31}$$

t_t is the equivalent disk thickness defined in Eq. (24) and $f_t = t_t / r_m$. Using the solid angle cone formula the number of liths attached around a layer surrounding the core can be evaluated with the following formula where the lith number is rounded off to the nearest integer:

$$N_l = O_{vl} \frac{2}{\left(1 - \sqrt{1 - \left(\frac{r_m}{r_s}\right)^2}\right)} \tag{32}$$

The total number is obtained by simply summing over the layers. The overlap factor can also account for the occurrence of partial cover in the outermost layer. For a ratio of coccolith radius to sphere radius of ½ which is approximately the case for the values used in this paper the number of coccoliths in the first layer is close to 15 [24].

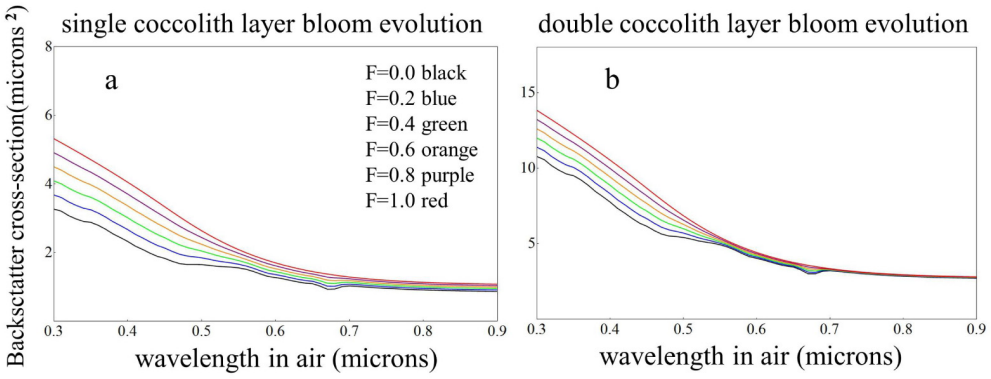

Fig. 7. Compound bloom spectral signatures (a) for a core covered with a single layer of liths at the start of shedding, and (b) for a core with two layers of liths at the start of shedding. The coccolith size distribution was modeled as a shifted Gamma function with a mean diameter of 2.4 microns and a standard deviation of 0.23 microns.

Figure 7 shows the results for the predicted spectral evolution of a bloom that starts with a single or a double layer of liths. As the bloom forms and the coccolithophores accrue multiple layers of liths a strong increase in light backscattering is seen. As the coccoliths are shed by the coccolithophores, the backscatter increases again but not as much. This effect is due to a close match between the geometric cross-section of a completely coated coccolithophore compared to that of the total cross-section of its free floating coccoliths, a fact already noted by Gordon et al. [24] during an *Ehux* bloom in waters of the Gulf of Maine. Note that the present simple model assumes no dynamics other than a transfer of a total fixed number of coated coccoliths into a corresponding ensemble of detached coccoliths and that both stay in the same volume for the entire time that the shedding takes place.

The average backscattering coefficient due to *Ehux*, $b_{bc}(\lambda)$ can be obtained from the results shown in Fig. 7 by multiplying the backscattering cross-section by the initial number density of coccolithophores in the bloom before shedding occurs. For typical blooms as analyzed in [24] the number density is on the order of $5\text{x}10^9$ m^{-3}. The absorption coefficient due to *Ehux*, $a_c(\lambda)$, can be obtained analogously. The resulting effect on the spectral remote-sensing reflectance $R_{rs}(\lambda)$ which is, to first order, proportional to the ratio of $b_b(\lambda)$ to $a(\lambda)+b_b(\lambda)$ [27], can be evaluated by adding $b_{bc}(\lambda)$ to the backscattering of the other standard water constituents to give total $b_b(\lambda)$ and by adding the $a_c(\lambda)$ due to the

Optics EXPRESS

coccolithophore cores to the total $a(\lambda)$. The results can be used to predict the effect of *Ehux* on the remote sensing reflectance either through a simple water albedo model such as that mentioned above or with more sophisticated modeling codes.

6. Conclusions and perspectives

We have derived an analytical model that captures the main features of light backscattering from coccoliths and coccospheres of the calcifying phytoplankter *Emiliania huxleyi*. We accounted for the morphological features of *Ehux* coccoliths and coccospheres detailed in previous work. Our model results for backscattering efficiency factors as a function of particle size and light wavelength matched closely with those from an exact ADA scattering code including the cases where abrupt transitions in scattering magnitude occurred. Our analytical model results for backscattering cross-section compared favorably to available in situ and laboratory data. We have also outlined an approach to predict the evolution of the magnitude and spectral behaviour of the backscattering coefficient during a bloom as *Ehux* sheds its liths as observed in natural waters and lab cultures. However as a note of caution we must mention that the fine-scale morphological features of real *Ehux* coccoliths (e.g., Fig. 1) are similar but not identical to those used in this study. Future work will incorporate the features of coccospheres and coccoliths of varying morphology and size distribution as derived from scanning electron microscopy images from in situ *Ehux* samples. We anticipate that this will bring our model even closer to reality and will allow us to accurately predict the effect of *Ehux* blooms on and ocean colour remote sensing reflectance. These efforts will allow us to improve space-borne and in situ optical algorithms for the estimation of coccosphere and coccolith abundance from backscattering, to develop strategies to optically differentiate coccospheres from coccoliths and to optically estimate coccolithophore bloom state.

Appendix

In this appendix we expand the expressions derived in the main part of the article to include the reflection of all the surfaces of both the coccolith and coccolithophore in the cases where absorption is present. When the imaginary index k is small relative to n we can use the following expression to account for the increase in the reflection coefficients due to its presence.

$$n_{eff} = 1 + \sqrt{(n-1)^2 + k^2} \tag{33}$$

We simply replace the indices in the formulas given in the main text of this paper by this effective index and use the anomalous diffraction approximation formulas for absorption efficiency with k as input to account for the attenuation between the surfaces. The coccolith disk geometry model used for the calculation of reflection coefficients is shown in Fig. 8 below.

Optics EXPRESS

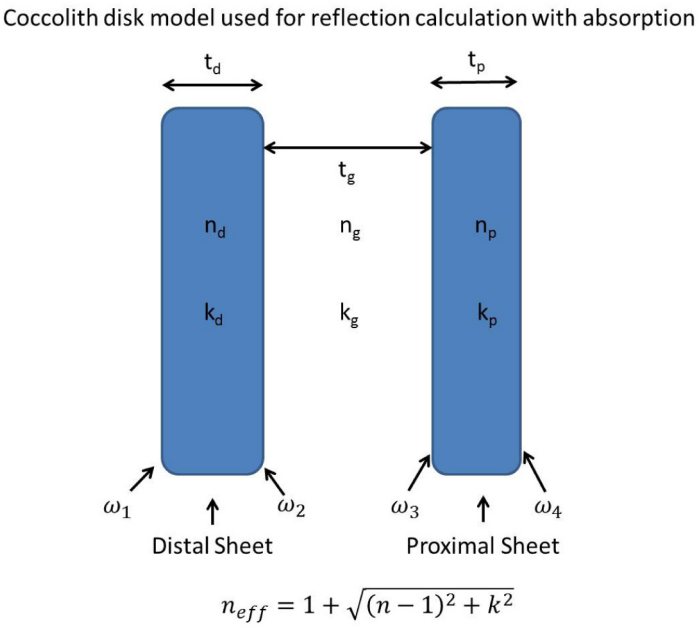

Fig. 8. Simple disk model of an *Emiliania huxleyi* coccolith used in this paper. The radii of both the distal and proximal sheets are equal to r_m in the full Zhai et al. [9] model shown in Fig. 2. The sum of their respective thicknesses, t_d and t_p, is equal to the total thickness t_t of a single disk of radius r_m that would contain the same volume of solid material as the actual complex Zhai coccolith shape. n_d , n_p and k_d, k_p denote the real and imaginary part of the refractive index of both distal sheets, respectively, while n_g and k_g denote the index of the gap between the sheets.

For the combination of the front four surfaces of a coccolith when absorption is present in the material we have for the total reflection term:

$$\begin{aligned}\omega_t &= \omega_1(n_d,k_d) + \omega_2(n_d,k_d)(1-\omega_1(n_d,k_d))(1-Q_{abs}(k_d,t_d))^2 \\ &+ \omega_3(n_d,k_d)(1-\omega_1(n_d,k_d))(1-\omega_2(n_d,k_d))(1-Q_{abs}(k_d,t_d))^2(1-Q_{abs}(k_g,t_g))^2 \\ &+ \omega_4(n_d,k_d)(1-\omega_1(n_d,k_d))(1-\omega_2(n_d,k_d))(1-\omega_3(n_d,k_d))(1-Q_{abs}(k_d,t_d))^2 \\ &(1-Q_{abs}(k_g,t_g))^2(1-Q_{abs}(k_p,t_p))^2\end{aligned} \tag{34}$$

and correspondingly for the backscatter reflection term:

$$\begin{aligned}\omega_{bsm} &= \omega_{b1}(n_d,k_d) + \omega_{b2}(n_d,k_d)(1-\omega_{b1}(n_d,k_d))(1-Q_{abs}(k_d,t_d))^2 \\ &+ \omega_{b3}(n_d,k_d)(1-\omega_{b1}(n_d,k_d))(1-\omega_{b2}(n_d,k_d))(1-Q_{abs}(k_d,t_d))^2(1-Q_{abs}(k_g,t_g))^2 \\ &+ \omega_{b4}(n_d,k_d)(1-\omega_{b1}(n_d,k_d))(1-\omega_{b2}(n_d,k_d))(1-\omega_{b3}(n_d,k_d))(1-Q_{abs}(k_d,t_d))^2 \\ &(1-Q_{abs}(k_g,t_g))^2(1-Q_{abs}(k_p,t_p))^2\end{aligned} \tag{35}$$

For randomly oriented disks we have derived a new absorption formula that is given by:

$$Q_{abs} = 1 + 2n^2\left[\left(\frac{n^2-1}{n^2}\right)E_3\left(2k\frac{2\pi t}{\lambda}\frac{n}{\sqrt{n^2-1}}\right) - E_3\left(2k\frac{2\pi t}{\lambda}\right)\right] \tag{36}$$

where E_3 the order 3 exponential integral function [28]. The corresponding Matlab codes are provided as supplementary material [18].

Optics EXPRESS

For the case of the coccolithophore we must evaluate the effect of both the coccolith surfaces on the front of the coccolithophore and from those on the back of the coccolithophore as the core of the coccosphere absorbs part of the light transmitted through the front coccoliths and reflected from the back coccoliths. For the front surfaces the expressions are the same as those for the coccoliths and for the back surfaces they are modified by the absorption of the intervening core of the coccosphere as follows:

$$Q_{bs} = Q_{bl} + Q_{bl}\left[1 - \left(\frac{r_c}{r_s}\right)^2 Q_{abs-sphere}\left(k_c, 2\,r_c\right)\right] \tag{37}$$

Where the absorption efficiency factor of the spherical core is given by:

$$Q_{abs-sphere}\left(k_c, r_c\right) = 2\left[\frac{1}{2} + \frac{e^{-\delta_c(\lambda)r_c}}{\delta_c(\lambda)r_c} + \frac{\left(e^{-\delta_c(\lambda)r_c} - 1\right)}{\left(\delta_c(\lambda)r_c\right)^2}\right] \tag{38}$$

Where

$$\delta_c(\lambda) = 4k(\lambda)\frac{2\pi}{\lambda} \tag{39}$$

Note that in the above expressions for absorption efficiency the wavelength in air should be used as the original measurements of $k(\lambda)$ were taken with reference to air wavelengths.

Funding

Griet Neukermans is funded by a Banting Postdoctoral Fellowship from the Government of Canada.

Acknowledgements

We would like to thank B. Ricard of DRDC for graciously having taken the time to create the scaled 3D model used in Fig. 2.We thank Dariusz Stramski [20] and Aimee Neeley [21] for providing the spectral absorption coefficient for an *Emiliania huxleyi* culture. We would also like to thank Emmanuel Boss and an anonymous reviewer for comments and suggestions that definitely helped improve our paper.